J Solid State Electrochem (2000) 4: 146–152

ORIGINAL PAPER

Ģirts Vītiņš · Zaiga Kaņepe · Aigars Vītiņš
Jānis Ronis · Antonija Dindūne · Andrejs Lūsis

Structural and conductivity studies in $LiFeP_2O_7$, $LiScP_2O_7$, and $NaScP_2O_7$

Received: 30 April 1999 / Accepted: 15 June 1999

Abstract Structural studies of $LiScP_2O_7$ by Rietveld refinement confirm that this material is isostructural with $LiFeP_2O_7$ studied previously. However, $NaScP_2O_7$ shows a structure different from the structural types of the basic group of $Na^IM^{III}P_2O_7$ known thus far. Systematic ranges for the six structural types of $A^IM^{III}P_2O_7$ are presented in terms of ion radii sums and ratios. The framework of $LiMP_2O_7$ (M = Sc, Fe) has rather wide tunnels running along the crystallographic *c*-axis. This feature has determined our interest to check the ion conductivity in $A^IM^{III}P_2O_7$ (A = Li, Na; M = Sc, Fe). The bulk conductivity, however, is low in these compounds, 10^{-6}–10^{-7} S/cm at 300 °C, as determined by impedance spectroscopy. In order to facilitate the conductivity via normal lithium sites, heterovalent substitution is used.

Key words Lithium scandium diphosphate · Lithium iron diphosphate · Sodium scandium diphosphate · Double diphosphates · Ion conductivity

Introduction

The double diphosphates $A^IM^{III}P_2O_7$ form cage structures where the framework is built of PO_4 tetrahedra and MO_6 octahedra sharing corners. The voids in the framework are occupied by monovalent cations with a distorted octahedral coordination, except for the small lithium ions which have a tetrahedral coordination. Six structural types can be distinguished among numerous double diphosphates $A^IM^{III}P_2O_7$, where A = Li, Na, K, Rb, Cs, Tl, and Ag and M = Al, Ga, transition metals, and some rare earth elements [1–12]. The structural types and corresponding examples are presented in Table 1. About 50 compounds for $A^IM^{III}P_2O_7$ have been checked for the structural type and the radii relations r_{A+M} and r_A/r_M are shown in Table 1. They allow us to see systematic ranges for at least the first three structural types. Structural type I represents the largest group of the $A^IM^{III}P_2O_7$ compounds. Characteristically, large A^+ ions (A = K, Rb, Tl, Cs) are involved in this structure. Type II represents a reduced number of the $A^IM^{III}P_2O_7$ compounds, where A are Na^+ and Ag^+ ions. However, a different structure is reported for $NaYP_2O_7$ single crystals [12]; in Table 1 its structure is denoted as a type VI. $NaYP_2O_7$ is the only representative of type VI and might be considered as an exception of type II. In structural type III two compounds, $LiFeP_2O_7$ [6, 7] and $LiMoP_2O_7$ [8], are thus far reported. Another one, $LiScP_2O_7$, we report in this paper. The framework of each of the first three structural types of $A^IM^{III}P_2O_7$ is determined by a particular arrangement of the six PO_4 tetrahedra, encompassing each MO_6 octahedron in a $[MP_6O_{23}]$ structural unit [6].

Structural types IV and V have their particular radii ranges as a subgroup within the ranges of the radii relations of structural type I. This indicates that the polymorphic transitions I-IV-V are possible for these compounds. Particularly, reversible polymorphic transitions are reported for $KErP_2O_7$, $KDyP_2O_7$ and $RbTbP_2O_7$ [3, 4]. Hamady et al. [5] have obtained full structural data on a single crystal of KYP_2O_7 representing structural type IV. The types of highest structural symmetry (IV and V) tend to appear at higher temperatures, when lattice vibrations are increased.

As is shown below, $LiFeP_2O_7$ and $LiScP_2O_7$ have straight and wide channels running along the crystallographic *c*-axis. These channels may serve for increased ion conductivity in $LiFeP_2O_7$ and $LiScP_2O_7$. Similarly, several other cage structures are known as sodium or lithium ion conductors, for instance $Na_3Zr_2Si_2PO_{12}$ (NASICON, conductivity at $\sigma_{300} = 0.14$ S/cm at

G. Vītiņš (✉) · A. Vītiņš · A. Lūsis
Institute of Solid State Physics, University of Latvia,
8 Kengaraga St., LV-1063 Riga, Latvia
e-mail: vitinsg@latnet.lv
Tel.: +371-7187817; Fax: +371-7112583

Z. Kaņepe · J. Ronis · A. Dindūne
Institute of Inorganic Chemistry, Riga Technical University,
34 Miera St., LV-2169 Salaspils, Latvia

Table 1 The six structural types of $A^{I}M^{III}P_2O_7$ reported previously

Type	Compound	Space group	r_{A+M}[a] (Å)	r_A/r_M[a]	Z	Unit cell parameters
I	$KAlP_2O_7$	$P\,2_1/c$	2.05–2.73	1.51–2.77	4	a = 7.308(8), b = 9.662(6), c = 8.025(4) Å; β = 106.69° [1, 9–11]
II	$NaAlP_2O_7$	$P\,2_1/c$	1.68–2.73	1.24–1.80	4	a = 7.197(2), b = 7.695(2), c = 9.312(2) Å; β = 111.73° [1, 2, 9]
III	$LiFeP_2O_7$	$P\,2_1$	1.34–1.47[b]	0.81–0.97[b]	2	a = 4.825(1), b = 8.079(2), c = 6.938(2) Å; β = 109.38° [5, 7, 8]
IV	$KErP_2O$	*Cmcm*	2.40–2.56	1.49–1.61	3	a = 5.704(2), b = 9.195(3), c = 12.216(5) Å [3–5]
V	$KTbP_2O_7$	n/a	2.40–2.43	1.48–1.53	6	a = 9.946(5), c = 12.822(2) Å [3, 4]
VI	$NaYP_2O_7$	$P\,2_1$	2.04	1.13	4	a = 7.004(1), b = 5.3740(8), c = 8.691(1) Å; β = 110.18° [12]

[a] The ion radii given by Shannon [13] are used in the calculation. The radii are recalculated according to $r(O^{2-})$ = 1.32 Å [14]
[b] Lithium ion radius for tetrahedral coordination is used

300 °C, activation energy $E_a = 0.24$ eV at 250–400 °C [15–17]), $Na_4ZrSi_3O_{10}$ ($\sigma_{300} = 0.004$ S/cm, $E_a = 0.44$ eV [18]), γ-$Na_3Sc_2(PO_4)_3$ ($\sigma_{300} = 0.09$ S/cm, $E_a = 0.20$ eV [19]), $Li_3Sc_2(PO_4)_3$ ($\sigma_{300} = 0.02$ S/cm, $E_a = 0.93$ eV at 90–171 °C, 0.28 eV at 282–467 °C [19]), etc. Sufficiently wide bottlenecks in the channels and the presence of free interstices, energetically advantageous for ion delocalization, allow fast ion transport in these compounds and structures.

First reports on $LiScP_2O_7$ and $NaScP_2O_7$ by Kaŋepe and Konstant [20, 21] concerned the synthesis, chemical analysis, infrared spectroscopy, and thermal analysis of these two compounds, confirmed also by X-ray analysis. A two-step synthesis by a solid state reaction via $NH_4ScP_2O_7$ has been proposed [20, 21]. However, the data of the X-ray powder diffraction [20, 21] are of a poor quality, and structural analysis for $LiScP_2O_7$ and $NaScP_2O_7$ has not been reported thus far.

The present paper reports structural studies of $LiScP_2O_7$ and $NaScP_2O_7$. Particularly, $NaScP_2O_7$ is not isostructural with $NaAlP_2O_7$ (II) and $NaYP_2O_7$ (VI) and thus represents a new structural type among the $A^{I}M^{III}P_2O_7$ diphosphates. Studies on impedance and ion conductivity in $LiScP_2O_7$, $NaScP_2O_7$, and $LiFeP_2O_7$ are presented in this paper. In order to try to release the ion conductivity via vacancies, a heterovalent substitution has been used. Single phase compounds of $Li_{0.9}Sc_{0.9}Zr_{0.1}P_2O_7$ and $Li_{0.9}Fe_{0.9}Ti_{0.1}P_2O_7$ have been obtained for conductivity studies. The substitution was done in accordance with the ion radii for octahedral coordination [14] [vs. $r(O^{2-}) = 1.32$ Å] as follows: $r(Sc^{3+}) = 0.81$, $r(Zr^{4+}) = 0.78$, $r(Fe^{3+}) = 0.68$, $r(Ti^{4+}) = 0.67$ Å.

Experimental

Synthesis

The diphosphates were obtained by a two-step synthesis. In the first step, in order to obtain $NH_4MP_2O_7$ (M = Sc, Fe), the corresponding amounts of simple metal oxides and $NH_4H_2PO_4$ were mixed and heated for 24 h to 250–280 °C. In the second step, $A^{I}M^{III}P_2O_7$ (A = Li, Na) were prepared in a solid state reaction between $NH_4MP_2O_7$ and A_2CO_3. In this step the synthesis (sintering) temperature for $LiScP_2O_7$, $LiFeP_2O_7$, and $NaScP_2O_7$ was 1100–1180, 950, and 1050 °C, respectively. $LiSc_{0.9}Zr_{0.1}P_2O_7$ and $LiFe_{0.9}Ti_{0.1}P_2O_7$ were obtained analogously. The purity of the materials was confirmed by X-ray analysis. The pellets prepared for impedance measurements had a density in the range 70–90% of the theoretical value (d_x).

X-ray powder diffraction

The X-ray powder diffraction pattern for $LiScP_2O_7$ was obtained by means of the DRON-3 diffractometer (Bragg-Brentano geometry). Cu $K\alpha$ (Ni filter) radiation and a slow sweep by steps of $0.04° \times 2\theta$ were used to obtain data for the Rietveld refinement of the $LiScP_2O_7$ structure by the program SR5 [22–24]. Preliminary unit cell calculations were performed by the least squares refinement of reflection positions by the autoindexing program TREOR [25]. More accurate analysis and cell parameters for $NaScP_2O_7$ were obtained by profile matching using the program Full Prof 3.5 [26]. In this refinement, data (step 0.02°, 10–90° 2θ) collected on the PW3710 diffractometer were used. A diffracted beam monochromator and Cu $K\alpha$ radiation were used in this experiment. The zero point of the 2θ scale was always controlled.

Impedance measurements

In order to determine the conductivity of the materials, impedance measurements were performed on a Hewlett Packard 4194A impedance/gain-phase analyzer, which works as an autobalancing ac bridge [27] and allows us to gather complex impedance data in a frequency range from 100 Hz to 40 MHz. Owing to parasitic effects of the wires (inductance, errors), which limit the accuracy at high frequency, a maximum frequency 20 MHz was used. The parasitic inductance was compensated or counted off by the software, where necessary (particularly at low impedance, <200 Ω). The parallel capacitance of the wires was determined and also subtracted by the software. The amplitude of the ac signal was set in the range 10–500 mV, depending on the resistance of the material. The impedance measurements were performed in temperature range 200–720 °C in air, both increasing and decreasing the temperature. Ceramic pellets covered by electrode materials on their opposite sides were used for the two-probe measurements. Smeared graphite, or Pt paste, sintered at 850 °C, served as the electrodes.

Results and discussion

Structural studies on $LiScP_2O_7$ and $NaScP_2O_7$

A preliminary investigation of the $LiScP_2O_7$ X-ray diffraction data by the TREOR program indicated a monoclinic unit cell with features resembling the unit cell of $LiFeP_2O_7$. The intensities of the diffraction reflections also showed a structural resemblance between both of the compounds. Therefore a Rietveld refinement on the basis of $LiFeP_2O_7$ atom positions [7] was performed for

Table 2 X-ray powder diffraction pattern for $LiScP_2O_7$. Data from a Rietveld refinement[a]

h	*k*	*l*	d_{calc} (Å)	I/I_0 (%)
1	0	0	6.610	9
1	1	0	5.193	100
0	0	1	4.651	1
−1	0	1	4.604	1
0	2	0	4.197	7
0	1	1	4.068	23
−1	1	1	4.036	70
1	2	1	3.543	30
1	0	1	3.314	31
2	0	0	3.305	6
−2	0	1	3.263	3
0	2	1	3.116	14
−1	2	1	3.101	78
1	1	1	3.082	23
2	1	0	3.075	17
−2	1	1	3.041	36
1	2	1	2.601	6
2	2	0	2.596	18
1	3	0	2.576	4
−2	2	1	2.576	2
−1	0	2	2.470	3
0	3	1	2.397	2
−1	3	1	2.391	1
−1	1	2	2.369	1
2	0	1	2.346	8
0	0	2	2.325	7
−3	0	1	2.316	2
−2	0	2	2.302	2
2	1	1	2.259	17
0	1	2	2.241	2

[a] Space group $P\ 2_1$, $a = 7.021(2)$, $b = 8.393(3)$, $c = 4.940(1)$ Å, $\beta = 109.71(1)°$, $V = 274$ Å^3, $d_x = 2.74$ g/cm^3, $R_{exp} = 5.19$, $R_p = 7.43$, $R_B = 4.7$, $R_{wp} = 9.84\%$, GOF = 3.4

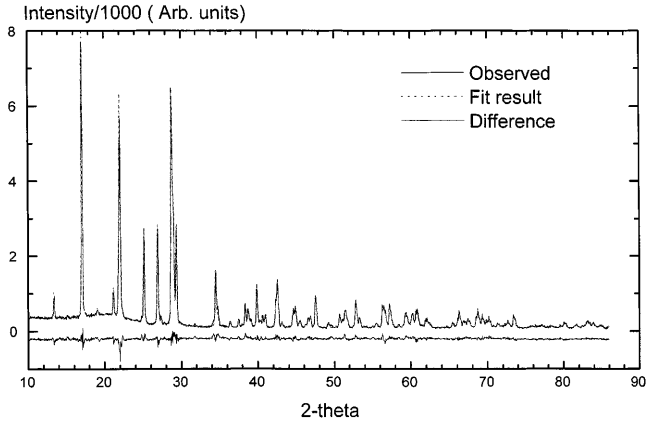

Fig. 1 X-ray powder diffraction pattern for $LiScP_2O_7$. Cu $K\alpha$ radiation was used. Experimental and calculated patterns, and the difference, are shown in the graph

Table 3 Refined atom positions for $LiScP_2O_7$

Atom	*x*/*a*	*y*/*b*	*z*/*c*	B^a (Å^2)
Li[b]	0.337(2)	0.365(2)	0.804(1)	1.9
Sc	0.268(1)	0.0000	0.791(1)	0.30
P(1)	0.473(1)	0.679(1)	0.592(1)	0.30
P(2)	0.080(1)	0.790(1)	0.205(2)	0.30
O(1)	0.130(2)	0.199(2)	0.884(3)	0.70
O(2)	0.401(2)	0.190(2)	0.600(3)	0.70
O(3)	0.496(2)	0.841(2)	0.762(3)	0.70
O(4)	0.072(2)	0.935(2)	0.388(3)	0.70
O(5)	0.115(2)	0.818(2)	0.925(3)	0.70
O(6)	0.497(2)	0.035(2)	0.194(3)	0.70
O(7)	0.232(2)	0.641(2)	0.384(3)	0.70

[a] Thermal factors *B* were not refined. *B* values close to the ones given for single-crystal $LiFeP_2O_7$ [7] were used
[b] Li positions, given for $LiFeP_2O_7$ [7], were not refined

the X-ray powder diffraction data of $LiScP_2O_7$. In the refinement, lithium positions and thermal factors were, however, not released, as they have little influence on the fit. A good fit was obtained in range 10–86° 2θ covering 240 theoretical reflections. Characteristics of the Rietveld refinement and of the X-ray diffraction pattern are given in Table 2. In the refinement, covering 240 theoretical reflections, the residual discrepancy *R* [28–31] is mainly determined by random errors, related to the quality of the collected diffraction data. As is seen in Fig. 1, the observed pattern follows the fit result pattern closely. The refined atom positions are listed in Table 3.

A check of the atom distances by the program Powder Cell [32] also indicates that the refinement is correct. The P-O distances are in range 1.499–1.686 Å with an average value 1.579 Å, corresponding to a radius 0.26 Å for P^{5+}, if the radius of the O^{2-} ion is 1.32 Å [13]. These values are close to 1.54 Å [2, 7] for P-O. The Sc-O distance [average 2.12 Å; $r(Sc^{3+}) = 0.80$ Å] in the ScO_6 octahedron is normal as well.

A drawing of the $LiScP_2O_7$ structure is shown in *ab*-plane projection in Fig. 2. There are straight and rather wide tunnels along the *c*-axis in the network built of the ScO_6 octahedra and the PO_4 tetrahedra sharing corners. Thus, the structure consists of identical layers piling up in the *c*-axis direction. The PO_4 tetrahedra are paired by

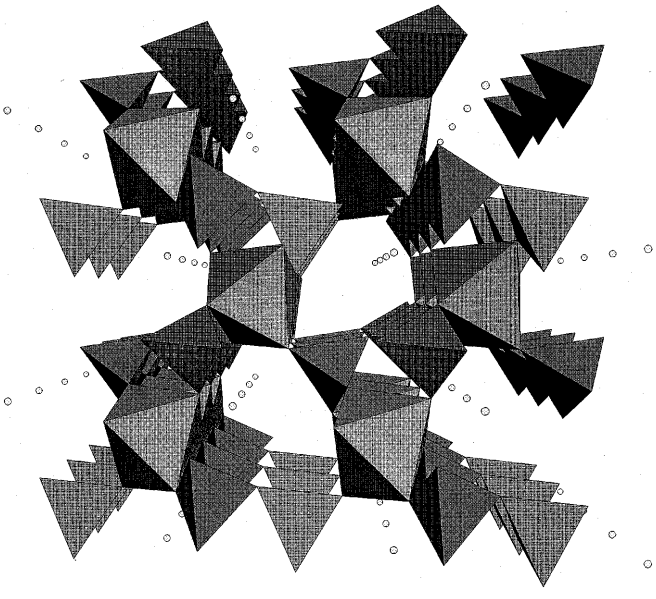

Fig. 2 A drawing of the $LiScP_2O_7$ structure in *ab*-plane projection. *Circles* are lithium ions of a reduced size

one corner forming the diphosphate anion $[P_2O_7]^{4-}$. The octahedron connected with two tetrahedra in the complex anion $[ScP_2O_7]^-$ serves as a basic unit of the structure. The bottlenecks in the tunnels along the *c*-axis are edged by four tetrahedra and two octahedra. Li^+ ions are located in the voids of the tunnels. Different from all the other metal ions involved in the formation of various $A^IM^{III}P_2O_7$ structural types considered, Li is coordinated by oxygen tetrahedrally in $LiScP_2O_7$ (as in $LiFeP_2O_7$). The mean Li-O distance in the distorted Li-O tetrahedron is 1.99 Å, corresponding to a Li^+ ion radius of 0.67 Å, if the O^{2-} radius is 1.32 Å.

The diffraction pattern of $NaScP_2O_7$ is shown in Fig. 3. A good fit has been obtained by the profile matching procedure. The fit using space group $P2_1$ confirms a monoclinic unit cell with a volume 566.7 Å^3. All the observed reflections have been indexed. An indexing of the line positions by a twice-reduced unit cell [$a = 8.484(1)$, $b = 5.306(1)$, $c = 6.715(1)$ Å, $\beta = 109.69(1)°$, $V = 284.7$ Å^3], similar to $NaYP_2O_7$ yielded a good merit [33] [$M(20) = 51$, $F(20) = 96$]. However, several significant lines of 2–5% intensity could not be indexed in this case. An attempt at a Rietveld refinement of the $NaScP_2O_7$ data on the basis of atom positions and symmetry of $NaYP_2O_7$ yielded an insufficient fit (GOF = 7, $R_{wp} = 19\%$, $R_{exp} = 8\%$ for all data) with the lines not matched. These lines have been tested as belonging to $NaScP_2O_7$. From the above we have to conclude that although there is a resemblance in structures between $NaYP_2O_7$ and $NaScP_2O_7$, these materials are not isostructural. Thus, the true characteristics of the X-ray powder diffraction of $NaScP_2O_7$ should be based on the large unit cell ($V = 566.7$ Å^3) as given in Table 4. These cell parameters and the diffraction pattern, however, are not isotypical for any of the six types of $A^IM^{III}P_2O_7$ (see Table 1) known until now. Although $NaScP_2O_7$ has $r_{A+M} = 1.89$ Å and $r_A/r_M = 1.33$, and thus relates to the range corresponding to structural type II, $NaScP_2O_7$ represents a new structural type (VII) among the $A^IM^{III}P_2O_7$ compounds. In order to determine the exact arrangement of its structure, single-crystal diffraction data are necessary.

Table 4 X-ray powder diffraction pattern of $NaScP_2O_7$. Data for profile matching by the Full Prof program[a]

h	*k*	*l*	d_{calc} (Å)	I/I_0 (%)
−1	0	1	7.978	13.0
1	0	1	6.314	4.0
2	0	0	6.040	8.0
0	1	1	4.509	0.6
2	0	1	4.457	0.6
−1	1	1	4.413	11.0
0	0	2	4.296	3.0
1	1	1	4.058	100.0
−2	0	2	3.988	57.0
3	0	1	3.348	4.0
0	1	2	3.337	29.0
−3	1	1	3.214	1.6
3	1	0	3.206	0.8
−2	1	2	3.186	6.0
−4	0	1	3.094	0.8
1	1	2	3.071	3.0
4	0	0	3.020	12.0
−1	0	3	2.952	4.0
−3	1	2	2.847	3.1
3	1	1	2.829	70.0
−4	0	2	2.813	35.0
2	1	2	2.712	3.0
−4	1	1	2.672	1.0
−3	0	3	2.659	3.0
4	0	1	2.654	1.4
0	2	0	2.649	24.0
1	0	3	2.646	14.0
4	1	0	2.623	13.0
1	2	0	2.587	4.0
−1	1	3	2.579	32.0
−2	1	3	2.525	1.8

[a] $a = 12.453(1)$, $b = 5.2970(6)$, $c = 8.857(1)$ Å, $\beta = 104.068(6)°$, $V = 566.7$ Å^3, $d_x = 2.84$ g/cm^3, $R_B = 1.3$, $R_P = 11$, $R_{wp} = 15$, $R_{exp} = 7.8\%$, GOF = 2.0

Conductivity studies on $LiScP_2O_7$, $LiFeP_2O_7$, and $NaScP_2O_7$

A typical form of the impedance spectra for different samples is represented in Fig. 4. The example of im-

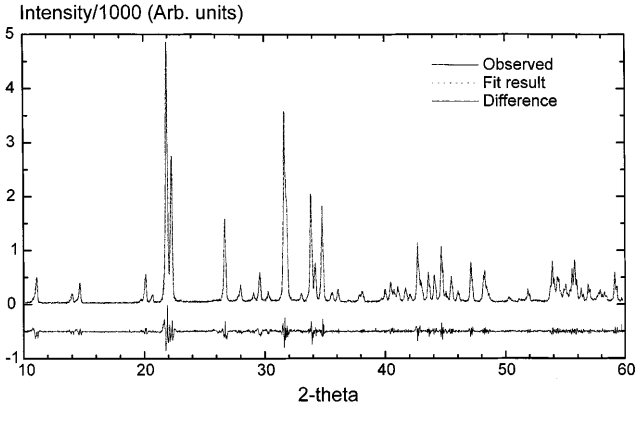

Fig. 3 X-ray powder diffraction pattern for $NaScP_2O_7$. Cu $K\alpha$ radiation was used. Experimental and calculated patterns, and the difference, are shown in the graph

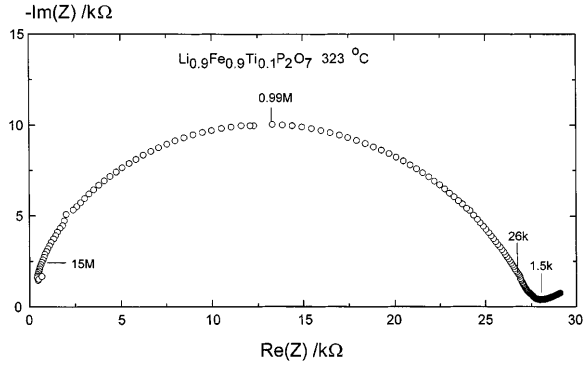

Fig. 4 An example of the impedance spectrum for $Li_{0.9}Fe_{0.9}Ti_{0.1}P_2O_7$. Numbers on the graph are the frequency in Hz

pedance data for $Pt/Li_{0.9}Fe_{0.9}Ti_{0.1}P_2O_7$ at 323 °C has the form of a somewhat depressed and distorted semicircle. Such a non-ideal form of the impedance semicircle is due to conductivity variation with frequency according to the jump relaxation model proposed by Funke [34] or according to a "universal dielectric response law" by Jonscher [35]. At low frequencies (below 1.5 kHz) a "tail" appears in the spectra, which corresponds to a contribution from the polarization on Pt electrodes. Simple data analysis confirms that the impedance semicircle corresponds to bulk properties of the material, as small capacities (10^{-12}–10^{-11} F/cm) determine the imaginary part of the semicircle. The relative dielectric permittivity is in the range 4–8 (at about 10–20 MHz), which is generally characteristic for inorganic oxide materials. The polarization at low frequency indicates that the compounds are ion conductors and the electron conductivity does not affect the impedance data in the frequency range used. Significant electronic conductivity in $A^{I}M^{III}P_2O_7$ (e.g., A = Li, Na; M = Sc, Fe) is not expected either, as the transition metal ions M^{3+} are separated (insulated) by $P^{5+}O_4$ tetrahedra in all the structural types mentioned, and the materials studied here are rather colorless. There should be a wide gap between the valence and conductivity zones in these materials.

The ionic conductivity of $NaScP_2O_7$, $LiScP_2O_7$, and $LiFeP_2O_7$ was found from the resistance obtained from the intersection of the impedance semicircle (see Fig. 4) on the real axis of the complex plane. Conductivity dependence on temperature is presented by plots of conductivity dependence against temperature in Fig. 5. The measurements on heating and cooling showed the effects of sorbed and bound water, if the materials were exposed in moist air. It is known that lithium salts tend to attract water. Thus, the conductivity is elevated by up to 1–2 orders. The effects of sorbed water on the conductivity disappear upon its evaporation. The sorbed water is lost at a rather high temperature of about 500–570 °C in the case of $LiFeP_2O_7$ and $LiScP_2O_7$. Similar effects, caused by sorbed water, were observed for the conductivity of $Li_{0.9}Fe_{0.9}Ti_{0.1}P_2O_7$ and $Li_{0.9}Sc_{0.9}Zr_{0.1}P_2O_7$. For the sake of simplicity, heating data for the conductivity of $LiScP_2O_7$ are not presented in Fig. 5. The heating and cooling data for the conductivity of $LiFeP_2O_7$ do not differ as the impedance of the sample was measured very soon after the heat treatment (850 °C) of the Pt electrode deposition. In the case of $NaScP_2O_7$, the effect of the sorbed water was observed up to 250–300 °C. The conductivity by protons from the sorbed water was controlled to be off and observation of the intrinsic conductivity by Li^+/Na^+ ions was ensured.

The alkali ion conductivity studied in lithium/sodium double diphosphates, is low and is in the range 10^{-7}–10^{-6} S/cm. Generally, from Fig. 5 it is seen that lithium ion conductivity is rather similar in both isostructural diphosphates, $LiFeP_2O_7$ and $LiScP_2O_7$. The conductivity plots for these two compounds do not take the shape of a single straight line according to the equation

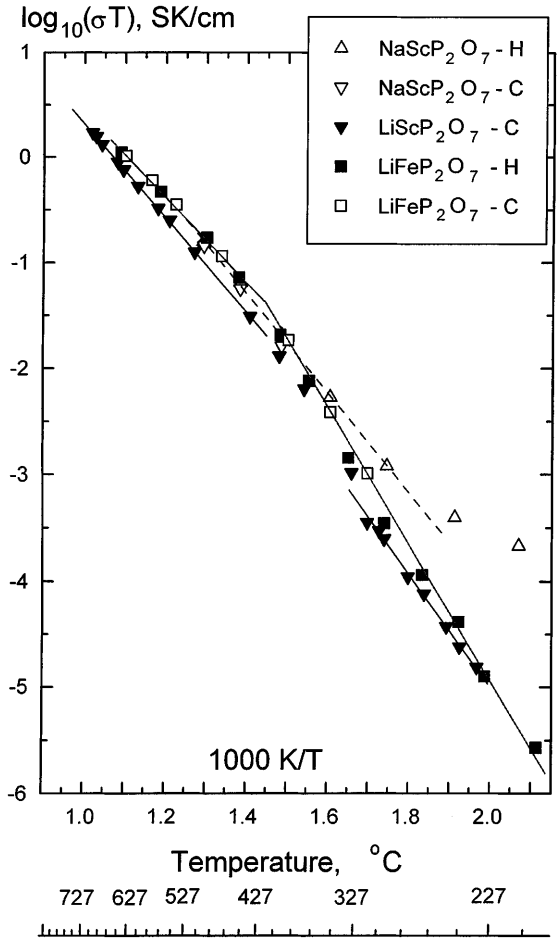

Fig. 5 Conductivity dependence on temperature for $NaScP_2O_7$, $LiScP_2O_7$, and $LiFeP_2O_7$. Heating (*H*) and cooling (*C*) data are shown

$$\sigma T = \sigma_0 \exp(-E_a/kT) \tag{1}$$

or Eq. (2) [36]. Instead, transitions in the conductivity occur at certain temperatures as the possible result of a sudden increase of charge carrier concentration (*Nc*) Eq. (2):

$$\sigma = \frac{\gamma N e^2 c(1-c) z a^2 \nu}{kT} \exp\left(\frac{\Delta S}{k}\right) \exp\left(-\frac{E_a}{kT}\right) \tag{2}$$

where γ is the correlation factor for the jumps, N is the total number of available sites per volume unit, e is the elementary charge, c is the fraction of mobile ions at these sites, z is the valence of charge carriers, a is the distance between the nearest sites, ν is the ion vibration frequency close to 10^{13} Hz, ΔS is the change of entropy, k is the Boltzmann constant, and E_a is the activation energy.

The plots of $LiFeP_2O_7$ and $LiScP_2O_7$ can be described by two regions of straight lines. Parameters for the plots of conductivity dependence on temperature are given in Table 5. The conductivity mechanism changes at about 320–350 °C for $LiScP_2O_7$ and at 417 °C for $LiFeP_2O_7$, whereas a single straight line fits the plot for

Table 5 Parameters for conductivity of double diphosphates investigated according to $\log(\sigma T) = \log \sigma_0 - 0.434 E_a/kT$

Compound	Density of d_x (%)	σ_{300} (S/cm)	$\log \sigma_0$	E_a (eV)	T range (C)
$LiScP_2O_7$	71	4×10^{-7}	5.6(2)	1.06(2)	250–320
			4.8(1)	0.89(1)	350–720
$Li_{0.9}Sc_{0.9}Zr_{0.1}P_2O_7$	90	2×10^{-5}	4.7(1)	0.77(1)	200–700
$LiFeP_2O_7$	76	8×10^{-7}	7.6(2)	1.23(2)	200–417
			4.4(1)	0.80(2)	417–650
$Li_{0.9}Fe_{0.9}Ti_{0.1}P_2O_7$	84	3×10^{-6}	5.4(1)	0.94(1)	194–303
			4.9(1)	0.81(1)	433–700
$NaScP_2O_7$	73	3×10^{-6}	5.3(2)	0.93(1)	250–470

$NaScP_2O_7$ in Fig. 5. Differential thermal analysis measurements have not indicated any notable thermal effects at the temperatures of transitions in conductivity. It seems that some kind of ion delocalization occurs above these transition temperatures and the activation energy of conductivity is reduced from 1.06 to 0.89 eV for $LiScP_2O_7$ and from 1.23 to 0.80 eV for $LiFeP_2O_7$ (see Table 5).

An extended analysis on the relation of conductivity to structure for $NaScP_2O_7$ is not possible as the exact structural arrangement in this material is unknown. In the case of $LiScP_2O_7$ and $LiFeP_2O_7$, the strong interaction between lithium and oxygen ions is the main factor limiting lithium ion transport, as the lithium ions are located in the sites of distorted tetrahedral coordination with rather short Li-O distances (about 0.67 Å). The localization is also determined by the low-polarizable surroundings and low-polarizable lithium ions themselves. Otherwise, there are a few conditions which may facilitate the ion transport in $LiScP_2O_7$ and $LiFeP_2O_7$. There are vacant tetrahedral positions near to the normal lithium sites. However, from the low conductivity in these materials we can conclude that these empty positions are not energetically advantageous. The bottlenecks along the c-axis are sufficiently wide (3.96 Å) for lithium ion transport, as they are close to the sum of the tetrahedral lithium ion diameter (1.30–1.34 Å) and the oxygen ion diameter (2.64 Å).

Although $LiScP_2O_7$ and $LiFeP_2O_7$ are isostructural, the materials show different features in the conductivity parameters presented in Table 5. The differences between both of the materials are due to the different ion radii: $r(Sc^{3+}) = 0.80$ and $r(Fe^{3+}) = 0.68$ Å. The shorter Fe-O distance provides the closer interaction between Fe and O than between Sc and O. Thus, it is expected that the charge from O is polarized towards Fe atoms. Therefore, the Li-O interaction should be released. Possibly, that explains the slightly lower activation energy for the conductivity in $LiFeP_2O_7$ than in $LiScP_2O_7$ at high temperatures. However, closer Fe-O interaction makes the framework of $[FeP_2O_7]^-$ more rigid. Possibly, this is a reason for the increased ion delocalization temperature (417 °C) and higher activation energy for conductivity in $LiFeP_2O_7$ at low temperatures. Otherwise, the bottlenecks of the tunnels in $LiFeP_2O_7$ are of the same width as in $LiScP_2O_7$.

The 10% substitution of Zr^{4+} for Sc^{3+} in $LiScP_2O_7$ yields an increase in the conductivity of 200 times and its activation energy is slightly reduced from 0.89 to 0.77 eV, as is seen in Table 5. For some reason the substitution of Ti^{4+} for Fe^{3+} is less effective as the conductivity increases only about 27 times. The increase in the conductivity is due to charge transport via vacancies in the normal lithium ion sites in the substituted compounds. The high activation energies for the conductivity (0.77–1.06 eV) in the substituted materials confirm that the lithium ions are strongly localized, being bonded with oxygen atoms in the low polarizable $[MP_2O_7]^-$ framework.

Conclusions

$LiScP_2O_7$ [$P\ 2_1$, $a = 7.021(2)$, $b = 8.393(3)$, $c = 4.940(1)$ Å, $\beta = 109.71(1)°$] is isostructural with $LiFeP_2O_7$, the type III $A^IM^{III}P_2O_7$ diphosphates, whereas $NaScP_2O_7$ has a structure different from the six types of $A^IM^{III}P_2O_7$ known thus far. In this way, $NaScP_2O_7$ [$a = 12.453(1)$, $b = 5.2970(6)$, $c = 8.857(1)$ Å, $\beta = 104.068(6)°$] appears as an exception, as according to the relations of the ion radii of Na^+ and Sc^{3+} it should show type II of $A^IM^{III}P_2O_7$ properties. Particularly, $NaScP_2O_7$ consists of ions similar to the ones involved in II-$NaInP_2O_7$.

Both diphosphates, $LiFeP_2O_7$ and $LiScP_2O_7$, show rather similar ion conductivity as they are isostructural. Although $LiFeP_2O_7$ and $LiScP_2O_7$ have a framework with sufficiently wide tunnels (bottlenecks of 3.96 Å) for lithium ion transport along the c-axis, the lithium ion conductivity in these materials is low. Similarly, low conductivity is observed for $NaScP_2O_7$. Different from, for instance, NASICON related structures, the frameworks of the diphosphates investigated do not provide conditions (empty energetically equivalent sites and released bonding of alkali ions within the framework) for ion delocalization and for fast ion conductivity.

We can conclude that low ion conductivity is expected in all the compounds of type III and in compounds related to the structure of $NaScP_2O_7$, if not in all the $A^IM^{III}P_2O_7$ system. Still, it might be interesting to test the conductivity in $AgM^{III}P_2O_7$ [1], where an effect of high-polarizable Ag^+ ions would be expected in the ion conductivity. We have also to conclude that the double diphosphates investigated are not in competition with several other fast Na^+/Li^+ ion conductors [e.g.,

$Li_3Sc_2(PO_4)_3$, NASICON, Na-β-alumina] applicable in ionic systems, for instance in sensors and batteries.

Acknowledgements The authors wish to thank Dr. K. West and his co-workers for arranging the X-ray powder diffraction of $NaScP_2O_7$ at the Department of Chemistry of the Technical University of Denmark.

References

1. Gabelica-Robert M, Tarte P (1983) New pyrophosphates $M^IM^{III}P_2O_7$. In: Mestselaar R, Heiligers HJM, Schoonman J (eds) Proc 2nd European conf on solid state chemistry, vol 3. Elsevier, Veldhoven, The Netherlands, pp 475–478
2. Gabelica-Robert M, Goreaud M, Labbe Ph, Raweau B (1982) J Solid State Chem 45: 389
3. Anisimova NYu, Chudinova NN, Trunov VK (1993) Neorg Mater 29: 106
4. Anisimova NYu, Chudinova NN, Trunov VK (1993) Neorg Mater 29: 104
5. Hamady A, Zid MF, Jouini T (1994) J Solid State Chem 113: 120
6. Genkina EA (1990) Zh Strukt Khim 31: 92
7. Genkina EA, Maksimov BA, Timofeva VA, Bykov AB, Mel'nikov OK (1985) Dokl Akad Nauk SSSR 284: 864
8. Ledain S, Leclaire A, Borel MM, Raveau B (1996) Acta Crystallogr C52: 1593
9. Gamondes JP, d'Yvoire F, Boullé A (1971) CR Acad Sci Paris 272C: 49
10. Nam Ng H, Calvo C (1973) Can J Chem 51: 2613
11. Yakubovich OV, Dimitrova OV, Strelkova EE (1995) Neorg Mater 31: 384
12. Hamady A, Jouini T (1996) Acta Crystallogr C52: 2949
13. Shannon RD, Previtt CT (1969) Acta Crystallogr B25: 925
14. Eucken A (ed) (1955) Zahlenwerte und Funktione aus Physik, Chemie, Astronomie, Gephysik und Technik, 6. I. Band: Atom- und Molekularphysik, 4. Teil: Kristalle. Springer, Berlin Heidelberg New York, pp 522–525
15. Goodenough JB, Hong HY-P, Kafalas JA (1976) Mater Res Bull 11: 203
16. Bayard ML, Barna GG (1978) J Electroanal Chem 91: 201
17. Bukun NG, Domashnev IA, Moskvina EI, Ukshe EA (1988) Neorg Mater 24: 447
18. von Alpen U, Bell MF, Höfer HH (1982) Solid State Ionics 7: 345
19. Bykov AB, Chirkin AP, Demyanets LN, Doronin SN, Genkina EA, Ivanov-Shits AK, Kondratyuk IP, Maksimov BA, Mel'nikov OK, Muradyan LN, Simonov VI, Timofeeva VA (1990) Solid State Ionics 38: 31
20. Kaŋepe Z, Konstant Z (1993) Latvian J Chem: 142
21. Kaŋepe Z, Konstant Z (1993) Latvian J Chem: 147
22. Wiles DB, Young RA (1981) J Appl Crystallogr 14: 149
23. Hill RJ, Howard CJ (1987) J Appl Crystallogr 20: 467
24. Madsen I, Hill RJ (1990) Powder Diffraction 5: 195
25. Werner P-E, Eriksson L, Westdahl M (1985) J Appl Crystallogr 18: 367
26. Rodriguez-Carvajal J (1993) Physica B 192: 55
27. Honda M (1989) A guide to measurement technology and techniques. Hewlett-Packard, Yokogawa, Japan
28. Rietveld HM (1967) Acta Crystallogr 22: 151
29. Rietveld HM (1969) J Appl Crystallogr 2: 65
30. Bérar JF, Lelann P (1991) J Appl Crystallogr 24: 1
31. Ståhl K (1994) Powder diffraction and the Rietveld method. University of Lund, Lund, pp 1–37
32. Kraus W, Nolze G (1996) J Appl Crystallogr 29: 301
33. De Wolf PM (1968) J Appl Crystallogr 1: 108
34. Funke K (1993) Prog Solid State Chem 22: 111
35. Jonscher AK (1975) Nature 253: 717
36. Goodenough JB (1978) Skeleton structures. In: Hagenmüller P, Van Gool W (eds) Solid electrolytes. Academic Press, New York, p 393